Electronic Supplementary Information

A first new porous *d-p* HMOF material with multiple active sites for excellent CO_2 capture and catalyst

Jiao Liu[a], Guo-Ping Yang*[a], Jing Jin[a], Dan Wu[a], Lu-Fang Ma[ab], and Yao-Yu Wang*[a]

[a]*Key Laboratory of Synthetic and Natural Functional Molecule Chemistry of the Ministry of Education, Shaanxi Key Laboratory of Physico-Inorganic Chemistry, College of Chemistry & Materials Science, Northwest University, Xi'an, 710127, Shaanxi, P. R. China. E-mail: ygp@nwu.edu.cn; wyaoyu@nwu.edu.cn.*

[b]*College of Chemistry and Chemical Engineering, Henan Key Laboratory of Function-Oriented Porous Materials, Luoyang Normal University, Luoyang 471934, P. R. China.*

Experimental section

Materials and Measurements. Unpurified materials were purchased. C, H and N were tested by Perkin-Elmer 2400C elemental analyzer. Infrared spectra (IR) were carried out Bruker EQUINOX-55 spectrophotometer in 4000–400 cm^{-1} region. Powder X-ray diffraction data (PXRD) were measured by Bruker D8 ADVANCE X-ray powder diffractometer. Thermogravimetric analyses (TGA) were determined by NETZSCH STA 449C microanalyzer thermal analyzer in N_2 protection atmosphere. Gas sorption isotherms were performed on ASAP 2020 M sorption equipment. ^1H NMR spectrograms were gained on a Bruker Ascend 400 (400 MHz) spectrometer.

Crystal Structure Determination The single crystal X-ray diffraction were acquired on Bruker SMART APEX II CCD diffractometer which contained graphite monochromated MoKα radiation (λ = 0.71073 Å) by using ϕ/ω scan technique. The diffraction data were corrected for Lorentz and polarization effects, meanwhile, for empirical absorption based on multi-scan. The complexes were ensured by direct method and refined anisotropically on F^2 by a full-matrix least-squares refinement with the *SHELXTL* program. The disordered molecules were processed by employing the SQUEEZE program of PLATON. The crystallographic, selected bond lengths and angles data of two complexes were listed in Table S1 and Table S2. CCDC: 1961111-1961112.

Gas Sorption Measurements. Before testing the sorption data for CO_2 and CH_4, the HMOF **2** was soaked in dichloromethane (CH_2Cl_2) for three days, and the activated sample was then heated under vacuum.

Catalytic Experiment. In the solvent-free environment, epoxide substrates with different sizes of substituted groups were used as reactants to react with CO_2, the activated **2** as catalysts and tetra-n-*tert*-butylammoniumbromide (TBAB) as co-catalyst. The catalytic reaction was carried out in a 5 mL Schlenk tube under stirring for 4 h (800rpm).

Synthesis process

Synthesis of $\{[Pb_2(L)_2(H_2O)]\cdot H_2O\}_n$ (1). A mixture of $Pb(NO_3)_2$ (0.1 mmol), H_2L (0.05 mmol), H_2O (3 mL), NMP (4 mL) and DMA (1 mL) were mixed in 15 mL Teflon-lined stainless steel vessel, and then heated at 120 °C for 72 h. After that the vessel cooled to room temperature with a rate of 10 °C h^{-1}, at last the colorless block crystals were obtained. Yield 94% (based on H_2L). Elemental analysis of **1**, calculated (%): C, 29.59; H, 1.58; N, 6.27. Found: C, 29.31; H,

1.54; N, 6.21. FT-IR (KBr, cm^{-1}, Fig. S6): 3532 (m), 3131 (w), 1514 (s), 1442 (m), 1249 (m), 1078 (m), 849 (m), 816 (w), 772 (m), 564 (w)

Synthesis of {[PbZn(L)$_2$]·DMA·H$_2$O}$_n$ (2). Mixture of **1** (0.03 mmol), $Zn(NO_3)_2·H_2O$ (0.6 mmol) and the same solvents of **1** were mixed in 15 mL Teflon-lined stainless steel vessel, and then heated at 120 °C for 72 h. After that the vessel cooled to room temperature with a rate of 10 °C h^{-1}, at last the colorless block crystals were obtained. Yield 76% (based on H_2L).

Moreover, under the same condition, the mixture of $Pb(NO_3)_2$ (0.05 mmol), $Zn(NO_3)_2·H_2O$ (0.05 mmol) and H_2L (0.05 mmol, 11.6 mg) was reacted to isolate the HMOF **2**. Yield 91% (based on H_2L). Elemental analysis of **2**, calculated (%): C, 35.1; H, 1.87; N, 7.46. Found: C, 34.8; H, 1.76; N, 7.41. FT-IR (KBr, cm^{-1}, Fig. S7): 3429 (m), 3148 (w), 1522 (w), 1427 (m), 1369 (m), 1249 (m), 1095 (m), 830 (w), 752 (m), 658 (w), 590 (w) .

Table S1. Crystal Data and Structure Refinements for **1**-**2**

Complex	**1**	**2**
Empirical formula	$C_{22}H_{14}N_4O_9Pb_2$	$C_{22}H_{14}N_4O_9PbZn$
Formula mass	892.75	750.93
Crystal system	Triclinic	Triclinic
Space group	*P-1*	*P-1*
a [Å]	10.489(3)	10.1986(4)
b [Å]	11.331(3)	12.0740(5)
c [Å]	11.564(3)	13.1106(6)
α [º]	90.053(4)	112.525(10)
β [º]	107.913(5)	91.216(10)
γ [º]	103.473(4)	95.011(10)
V [Å^3]	1267.9(6)	1482.93(11)
Z	2	2
$D_{calcd.}$[g·cm^{-3}]	2.339	1.682
μ [mm^{-1}]	13.319	6.527
F [000]	820	716
θ [º]	1.854 - 24.999	2.544 – 24.998
Reflections collected	6251 / 4382	33680 / 5217
Goodness-of-fit on F^2	1.037	1.026
Final *R*[a] indices [I>2σ(I)]	R_1 = 0.0749 wR_2 = 0.2570	R_1 = 0.0204 wR_2 = 0.0656

[a] $R_1=\sum||F_o|-|F_c||/\sum|F_o|$, $wR_2=[\sum w(F_o^2-F_c^2)^2/\sum w(F_o^2)^2]^{1/2}$

Table S2. Selected bond distances (Å) and angles (º) for **1**-**2.**

Complex **1**			
Pb(1)-O(1)	2.327(14)	O(1)-Pb(1)-N(3)	75.7(5)
Pb(1)-N(3)	2.484(15)	O(1)-Pb(1)-O(5)#1	75.5(5)
Pb(1)-O(5)#1	2.517(17)	N(3)-Pb(1)-O(5)#1	102.9(5)
Pb(1)-O(4)#2	2.672(13)	O(1)-Pb(1)-O(4)#2	80.8(4)
Pb(2)-N(1)	2.375(15)	N(3)-Pb(1)-O(4)#2	81.7(5)
Pb(2)-O(3)#3	2.371(14)	O(5)#1-Pb(1)-O(4)#2	153.8(5)
Pb(2)-O(8)#4	2.481(15)	N(1)-Pb(2)-O(3)#3	77.5(5)
Pb(2)-O(9)	2.734(17)	N(1)-Pb(2)-O(8)#4	91.9(5)
O(3)-Pb(2)#3	2.371(14)	O(3)#3-Pb(2)-O(8)#4	81.0(5)
O(4)-Pb(1)#2	2.672(13)	N(1)-Pb(2)-O(9)	85.6(5)
O(5)-Pb(1)#1	2.517(17)	O(3)#3-Pb(2)-O(9)	69.9(5)
O(8)-Pb(2)#5	2.481(15)	O(8)#4-Pb(2)-O(9)	150.7(5)
Complex **2**			
Pb(1)-O(8)#1	2.314(3)	O(8)#1-Pb(1)-O(6)	87.32(10)
Pb(1)-O(4)#2	2.459(3)	O(4)#2-Pb(1)-O(6)	71.32(10)
Pb(1)-O(6)	2.496(3)	O(8)#1-Pb(1)-O(3)#2	92.62(11)
Pb(1)-O(3)#2	2.514(3)	O(4)#2-Pb(1)-O(3)#2	52.13(9)
Pb(1)-O(3)#3	2.677(3)	O(6)#2-Pb(1)-O(3)#2	122.40(10)
Zn(1)-O(1)	1.934(2)	O(8)#1-Pb(1)-O(3)#3	76.92(11)
Zn(1)-N(4)#4	1.992(3)	O(4)#2-Pb(1)-O(3)#3	113.59(9)
Zn(1)-O(5)	2.001(3)	O(6)-Pb(1)-O(3)#3	162.02(10)
Zn(1)-N(2)#5	2.023(3)	O(3)#2-Pb(1)-O(3)#3	67.71(10)
O(3)-Pb(1)#2	2.514(3)	O(1)-Zn(1)-N(4)#4	118.75(12)
O(3)-Pb(1)#6	2.677(3)	O(1)-Zn(1)-O(5)	118.11(11)
O(4)-Pb(1)#2	2.459(3)	N(4)#4-Zn(1)-O(5)	110.91(13)
O(8)-Pb(1)#1	2.313(3)	O(1)-Zn(1)-N(2)#5	107.07(11)
N(2)-Zn(1)#5	2.023(3)	N(4)#4-Zn(1)-N(2)#5	103.38(12)
N(4)-Zn(1)#4	1.992(3)	O(5)-Zn(1)-N(2)#5	94.27(12)
O(8)#1-Pb(1)-O(4)#2	80.13(11)	Pb(1)#2-O(3)-Pb(1)#6	112.29(10)

Symmetry transformations used to generate equivalent atoms in **1**: #1: -x+2, -y, -z; #2: -x+2, -y+1, -z; #3: -x+3, -y+1, -z+1; #4: x+1, y, z; #5: x-1, y, z. Symmetry transformations used to generate equivalent atoms in **2**: #1: -x, -y+1, -z+1; #2: -x+1, -y+1,-z; #3: x-2, y, z; #4: -x, -y+2, -z+1; #5: -

x+1, -y+2, -z+1; #6: x+1, y, z.

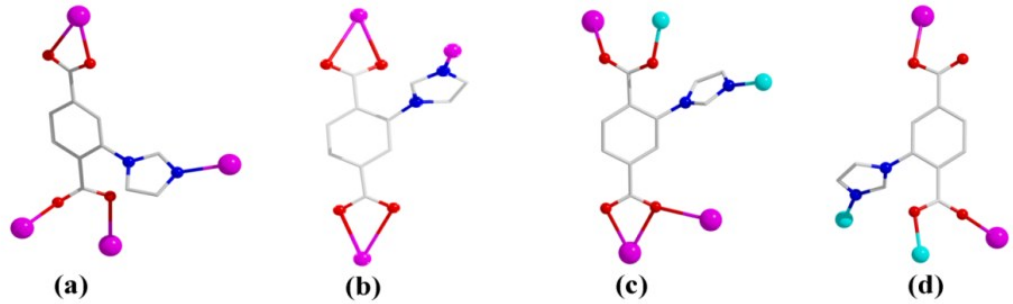

Fig. S1 The coordination modes of L^{2-} ligands in **1-2**.

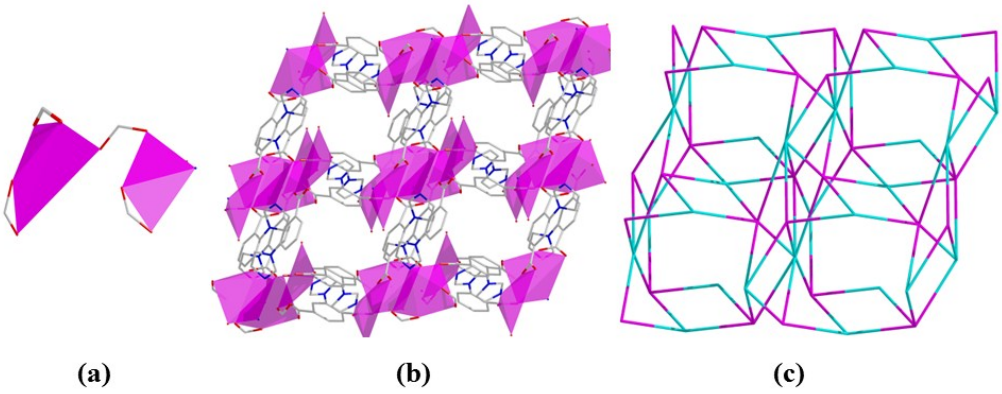

Fig. S2 (a) Two adjacent of Pb(II) ion viewed as an SBU of **1**. (b) 3D dense framework structure of **1**. (c) Topological net for **1**.

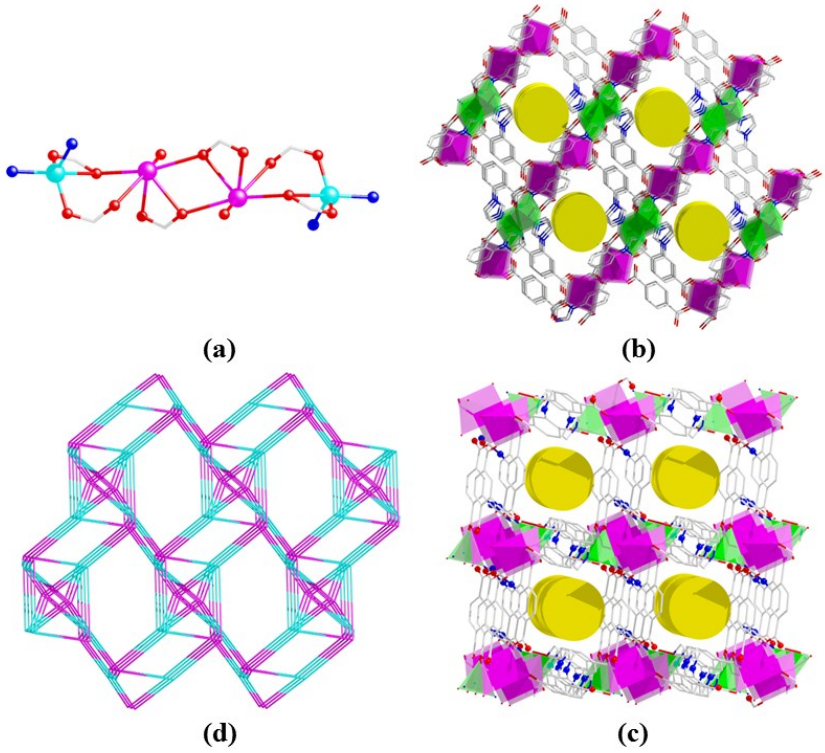

Fig. S3 The 1D rod-shaped SBU in **2** (a); the 3D porous framework of **2** along [722] axis (b) and

[177] axis (c), and the topological net for **2** (d).

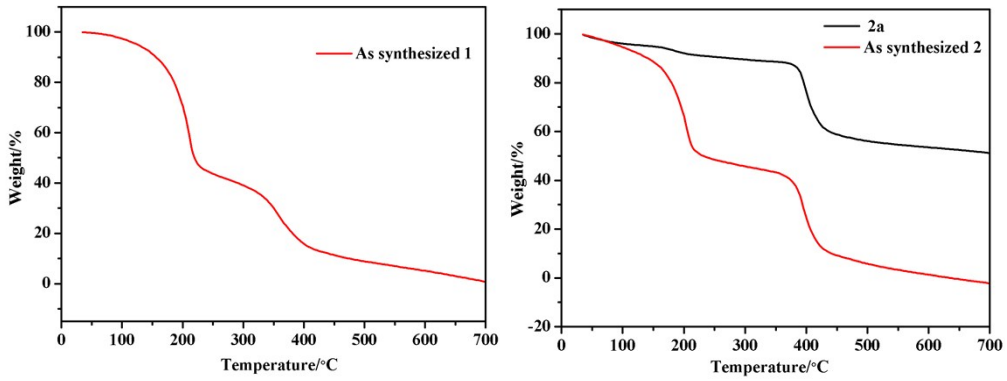

Fig. S4 The TGA curves for **1** and **2.**

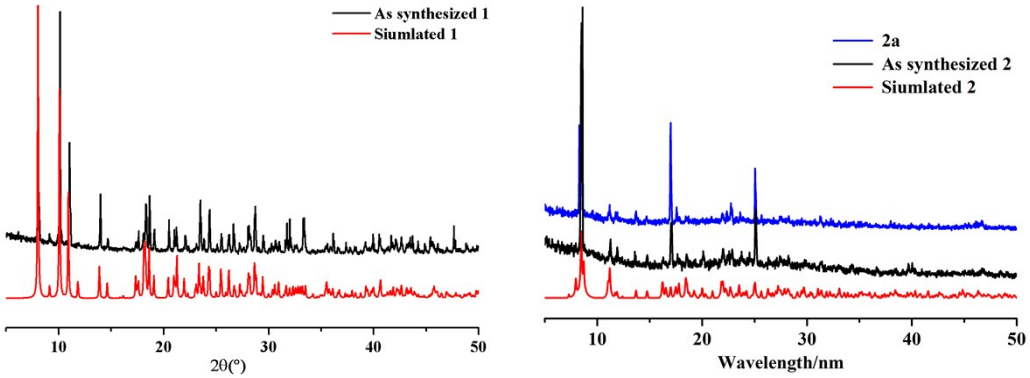

(a) **(b)**

Fig. S5 The PXRD patterns of the as-synthesized products **1** (a) and **2** (b).

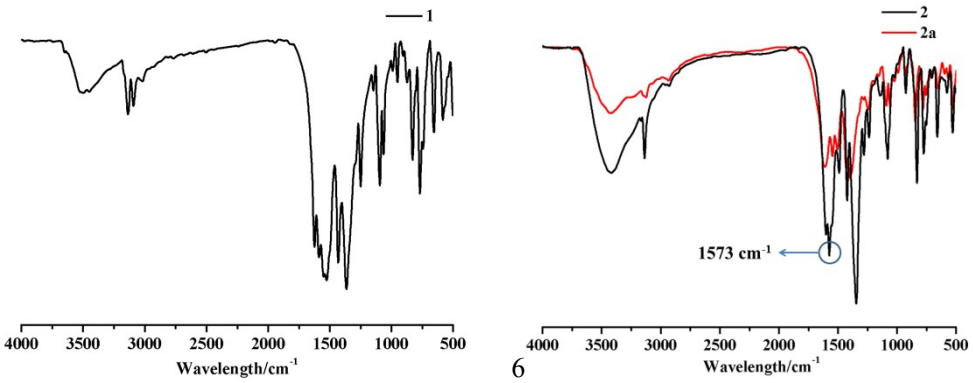

6

Fig. S6 The FT-IR spectra of the as synthsized **2** and desolvated **2** (**2a**). The characteristic C=O vibration at 1573 cm^{-1} of DMA in **2a**, indicating the removal of DMA molecules.

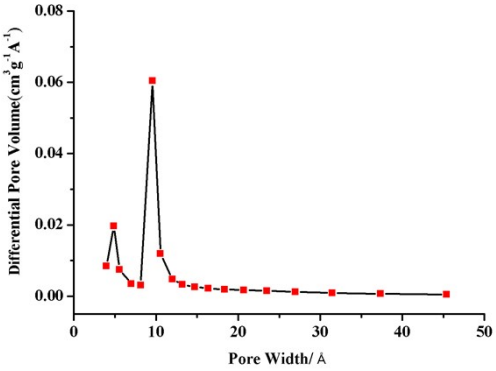

Fig. S7 PSD obtained from the 195 K isotherms using H-W mode.

The experimental isotherm data for pure CO_2 and CH_4 (measured at 273 and 298 K) were fitted using a Langmuir-Freundlich (L-F) model

$$\mathbf{q} = \frac{a * b * p^c}{1 + b * p^c}$$

Where q and p are adsorbed amounts and pressures of component i, respectively. The adsorption selectivities for binary mixtures of CO_2/CH_4 at 273 and 298 K., defined by

$$\boldsymbol{S_{ads} = (q1/q2)/(p1/p2)}$$

Where qi is the amount of i adsorbed and pi is the partial pressure of i in the mixture.

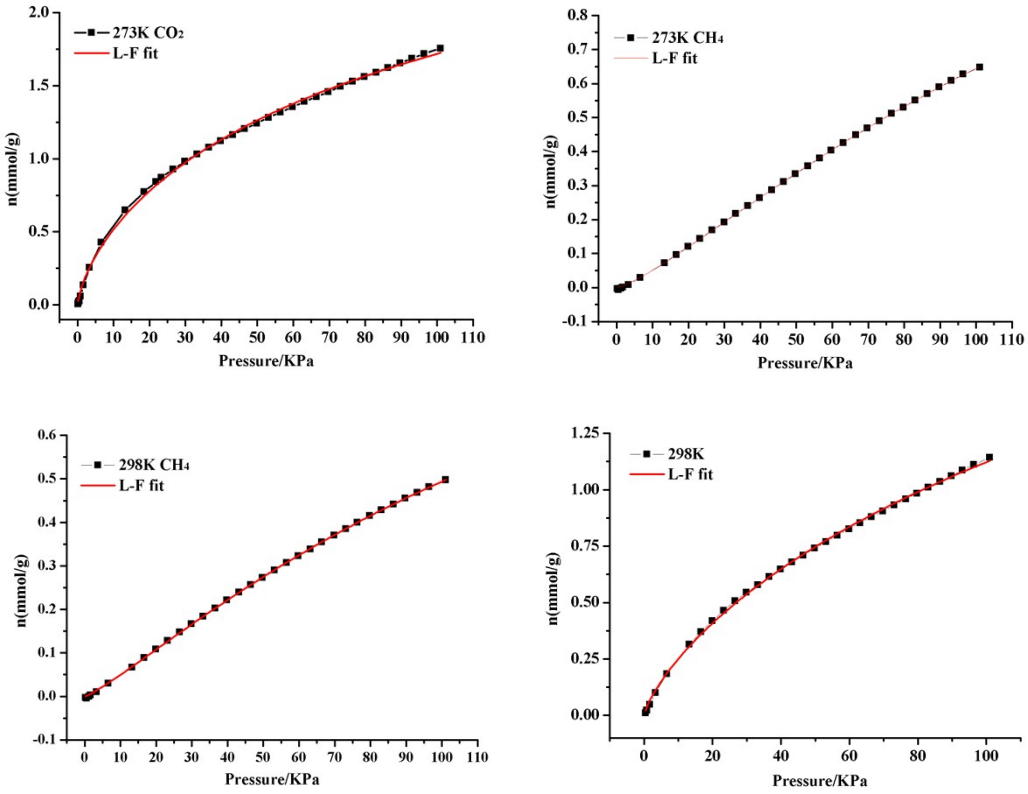

Fig. S8 CO_2 adsorption isotherms of **2a** at 273 K with fitting by L-F model: a = 3.97164, b = 0.02921, c = 0.70837, Chi^2 = 4.98434E-4, R^2 = 0.99848; CO_2 adsorption isotherms of **2a** at 298 K with fitting by L-F model: a = 3.93474, b = 0.01154, c = 0.7679, Chi^2 = 9.6559E-5, R^2 = 0.99923; CH_4 adsorption isotherms of **2a** at 273 K with fitting by L-F model: a = 1.7657, b =

0.00153, c = 1.28737, Chi^2 = 6.05926E-6, R^2 = 0.99987; CH_4 adsorption isotherms of **2a** at 298 K with fitting by L-F model: a = 1.32414, b = 0.00255, c = 1.18428, Chi^2 = 3.99026E-4, R^2 = 0.99985.

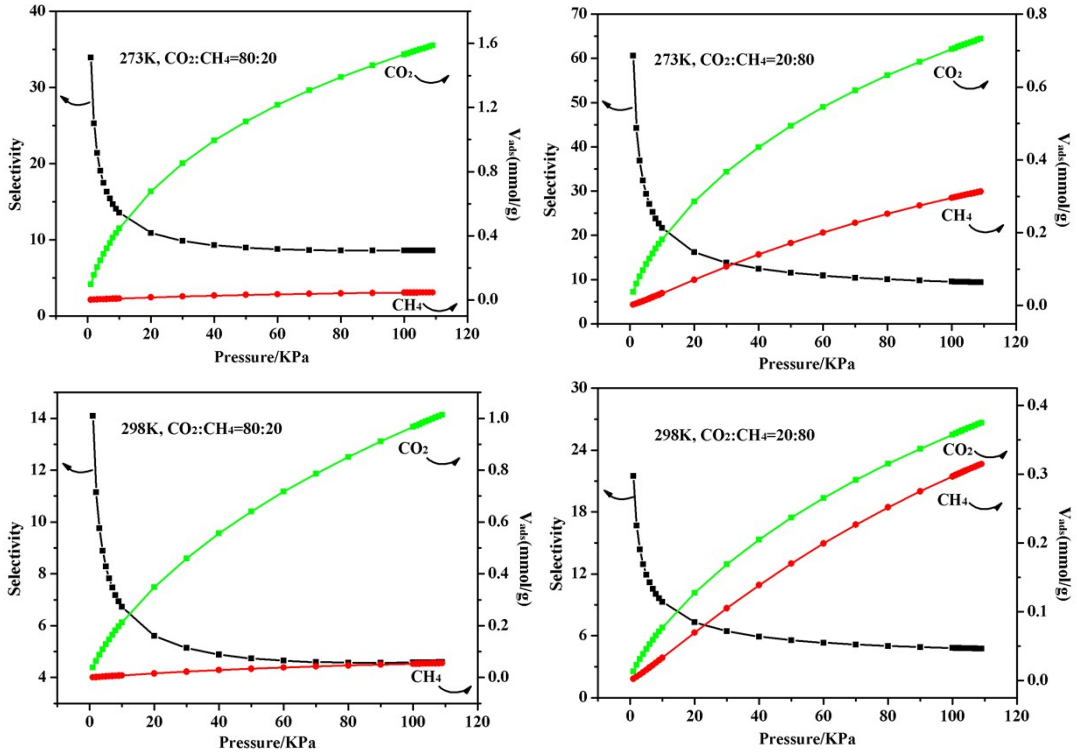

Fig. S9 IAST adsorption selectivity of **2a** for equimolar mixtures of CO_2 and CH_4 at 273 K and 298 K.

Calculation of sorption heat for CO_2 and CH_4 uptake using Virial 2 model

The CO_2 and CH_4 adsorption isotherm data for **2a** at 298 K were fitted using the Virial 2 expression, where P is the pressure, N is the adsorbed amount, T is the temperature, a_i and b_i are virial coefficients, and m and N are the number of coefficients used to describe the isotherms. Q_{st} is the coverage–dependent enthalpy of adsorption and R is the universal gas constant.

$$\ln P = \ln N + 1/T \sum_{i=0}^{m} a_i N^i + \sum_{i=0}^{n} b_i N^i \qquad Q_{st} = -R \sum_{i=0}^{m} a_i N^i$$

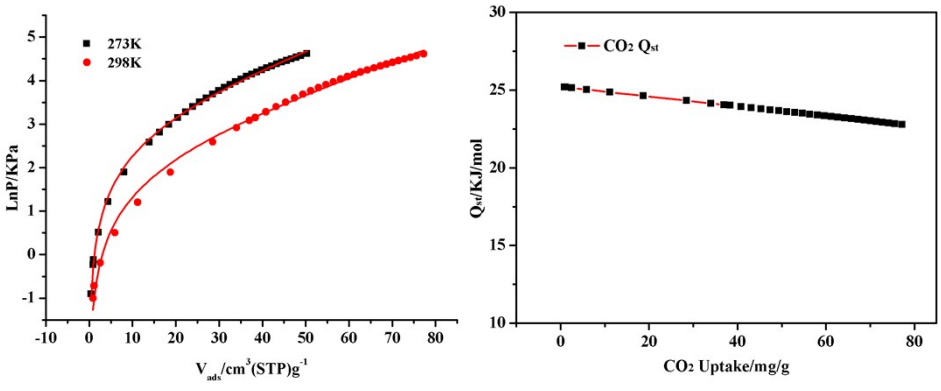

(a) **(b)**

Fig. S10 (a) CO_2 adsorption isotherms for **2a** with fitting by Virial 2 model. Fitting results: a0 = –3033.03469, a1 = 3.83436, a2 = 0.01513, b0 = -11.32327, b1 = 0.00254, Chi^2 = 0.00751, R^2 = 0.99681. (b) Isosteric heat of CO_2 adsorption for **2a** estimated by the virial equation from the adsorption isotherms 273 K.

Table S3 Comparison of CO_2 separation performances at 298 K of **2a** and other MOFs.

MOF	Selectivity	Ref.
ZJNU-63	3.5	1
Cu_2(pbpta)	6	2
[Ni(btzip)(H_2btzip)]·2DMF·2H_2O	13.9	3
{[$Cu_{0.5}$(bpdado)$_{0.5}$(bpe)$_{0.5}$]·3H_2O}$_n$	15.5	4
JLU-Liu18	4.5	5
JLU-Liu46	9.8	6
MIL-53(Al)	2.3	7
MOF-205-OBn	2.7	8
MFM-130a	7.1	9
[Me_2NH_2][Zn_2(BDPP)(HTZ)]·4DMF	4	10
{[PbZn(L)$_2$]·DMA·H_2O}$_n$	**16.2**	**This work**

Table S4 Comparison of CO_2 separation performances at 273 K of **2a** and other MOFs.

MOF	Selectivity	Ref.
ZJNU-63	4.2	1
Cu_2(pbpta)	12	2
ZJU-16	38	11
MFM-130a	9.4	9
ZIF-95	4.3	12
ZIF-100	5.9	12
HKUST-1	7.1	13
{[PbZn(L)$_2$]·DMA·H_2O}$_n$	**41.3**	**This work**

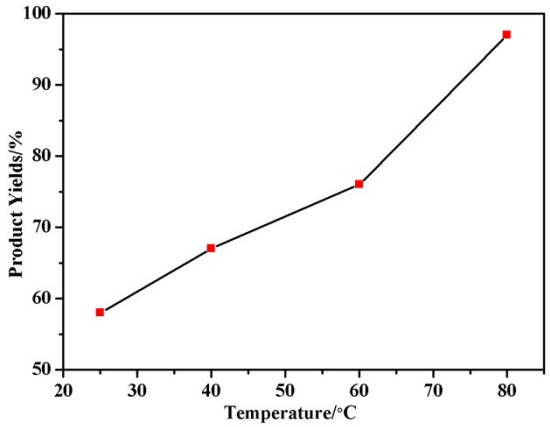

Fig. S11 The curve of the yields *versus* temperatures.

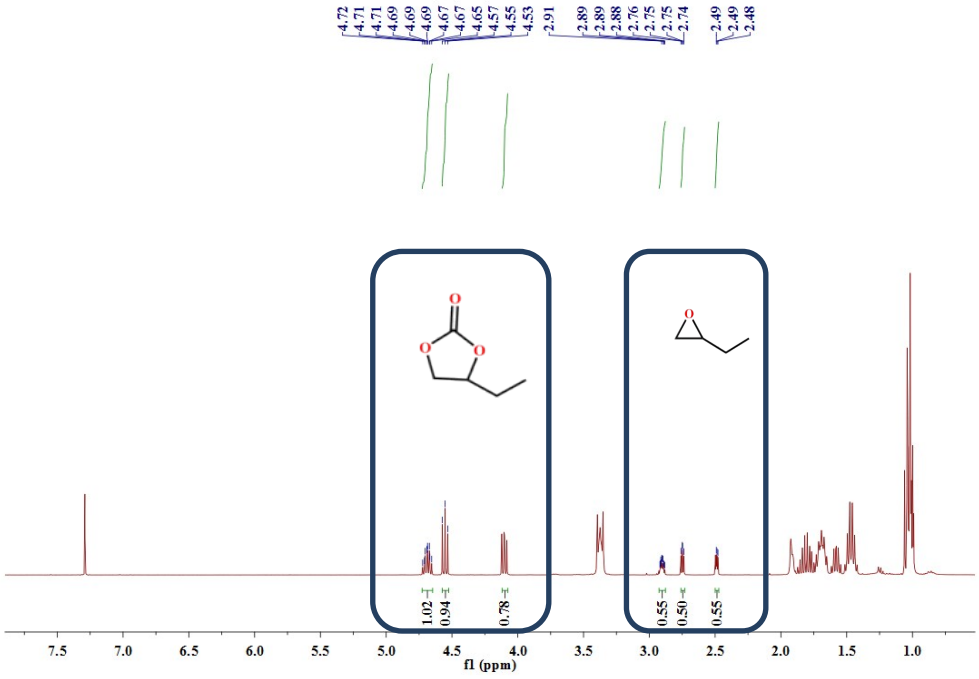

[1] H NMR spectrum of cyclic carbonate with **2a** (Table 1, entry 1).

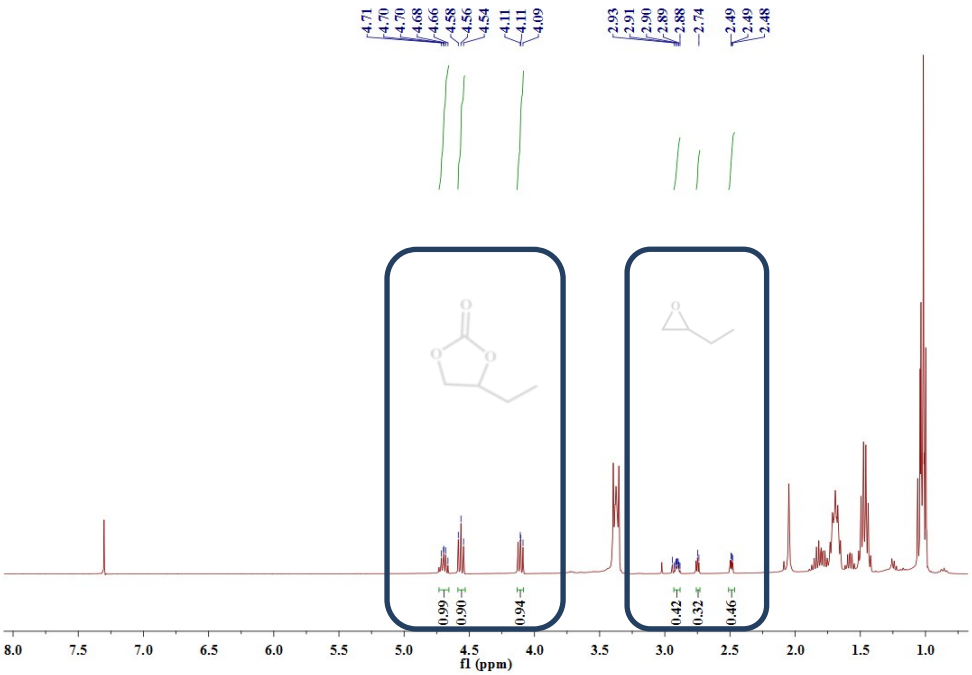

[1] H NMR spectrum of cyclic carbonate with **2a** (Table 1, entry 2).

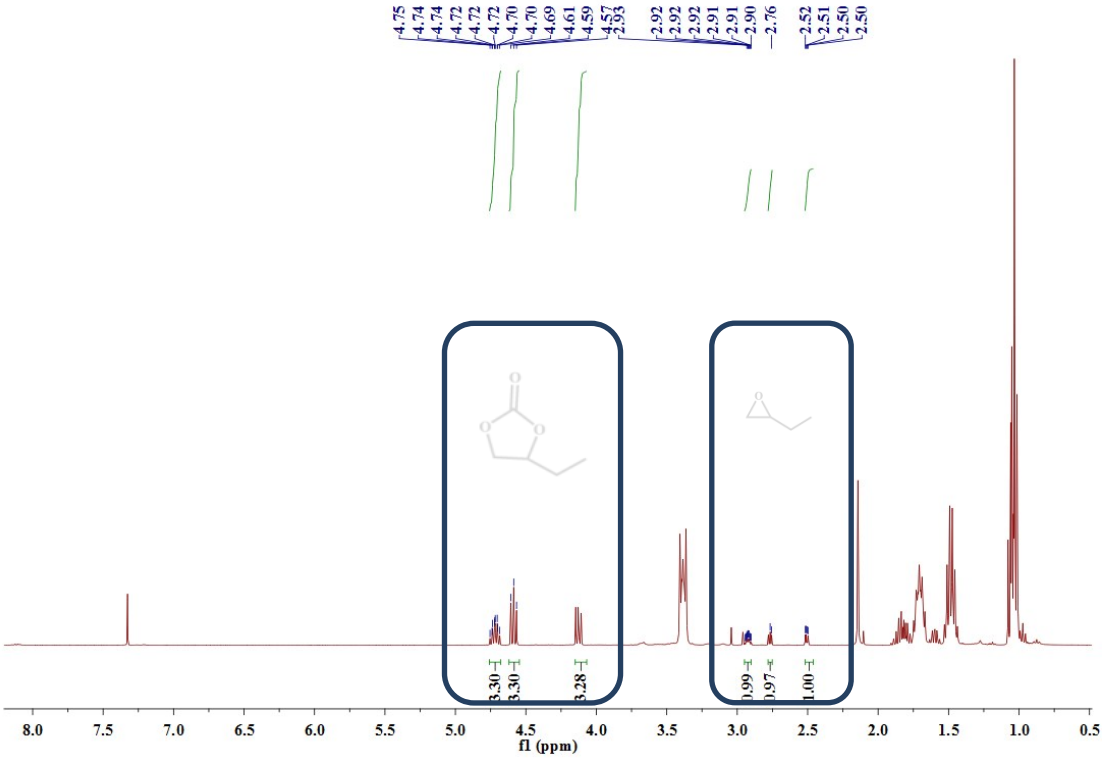

[1] H NMR spectrum of cyclic carbonate with **2a** (Table 1, entry 3).

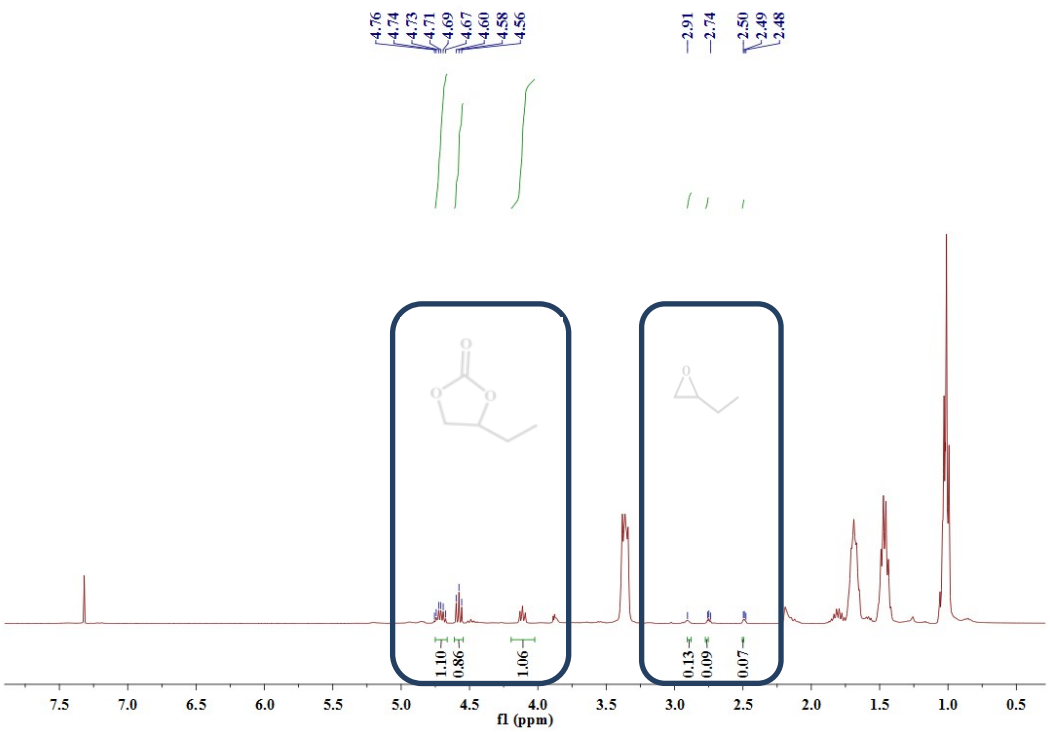

[1] H NMR spectrum of cyclic carbonate with **2a** (Table 1, entry 4).

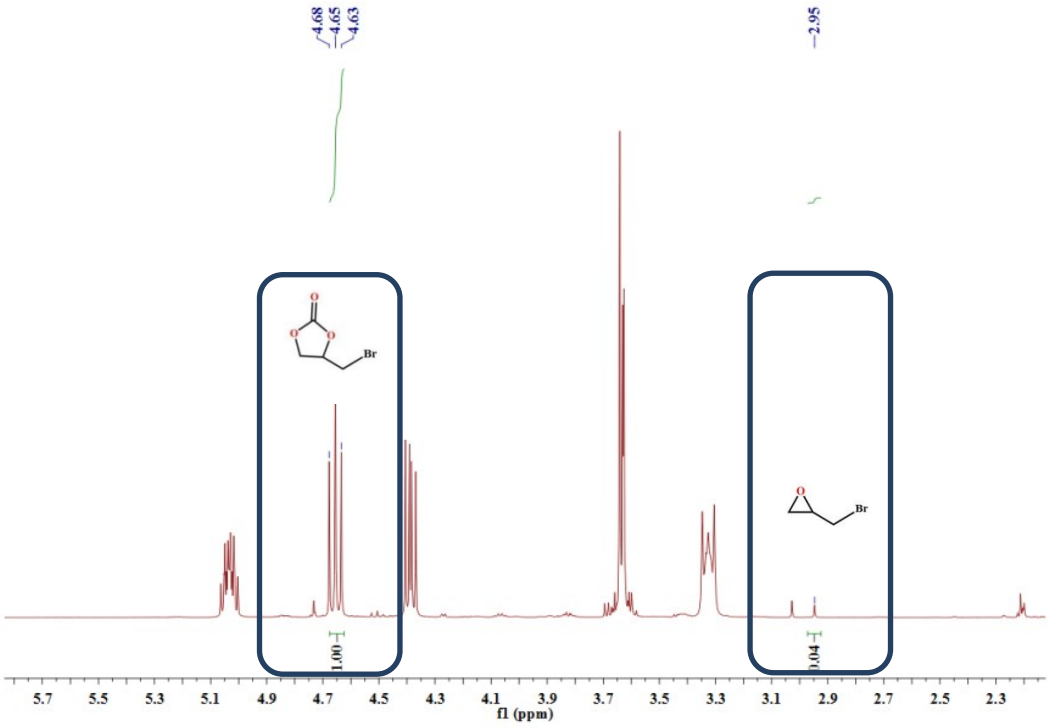

[1] H NMR spectrum of cyclic carbonate with **2a** (Table 1, entry 5).

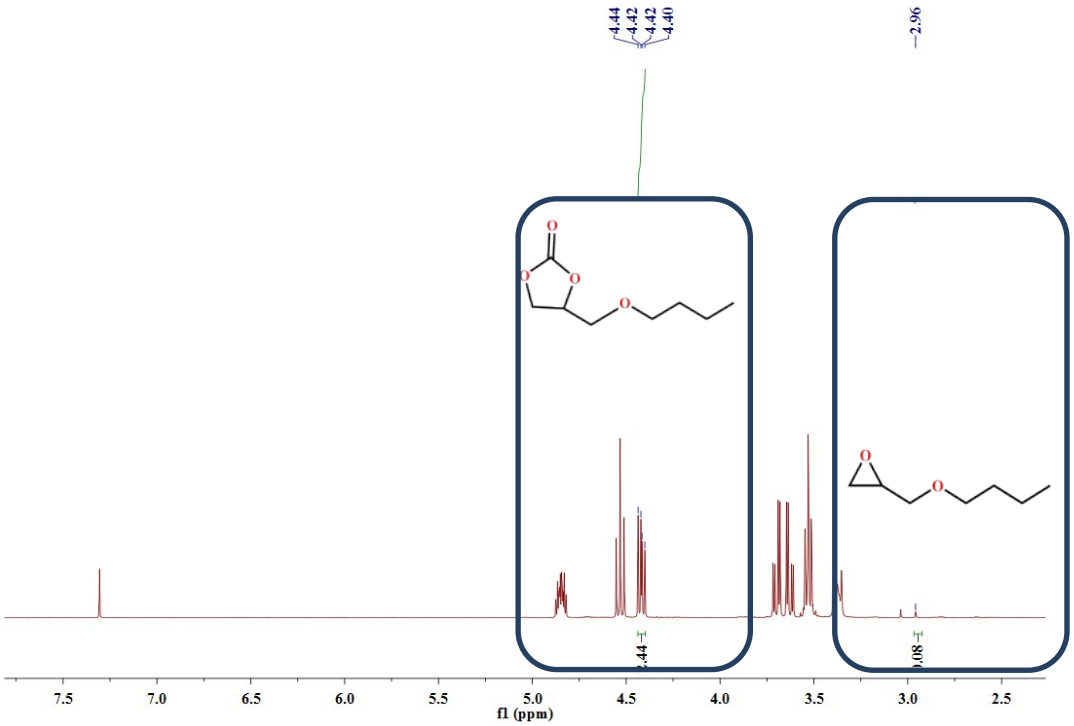

[1] H NMR spectrum of cyclic carbonate with **2a** (Table 1, entry 6).

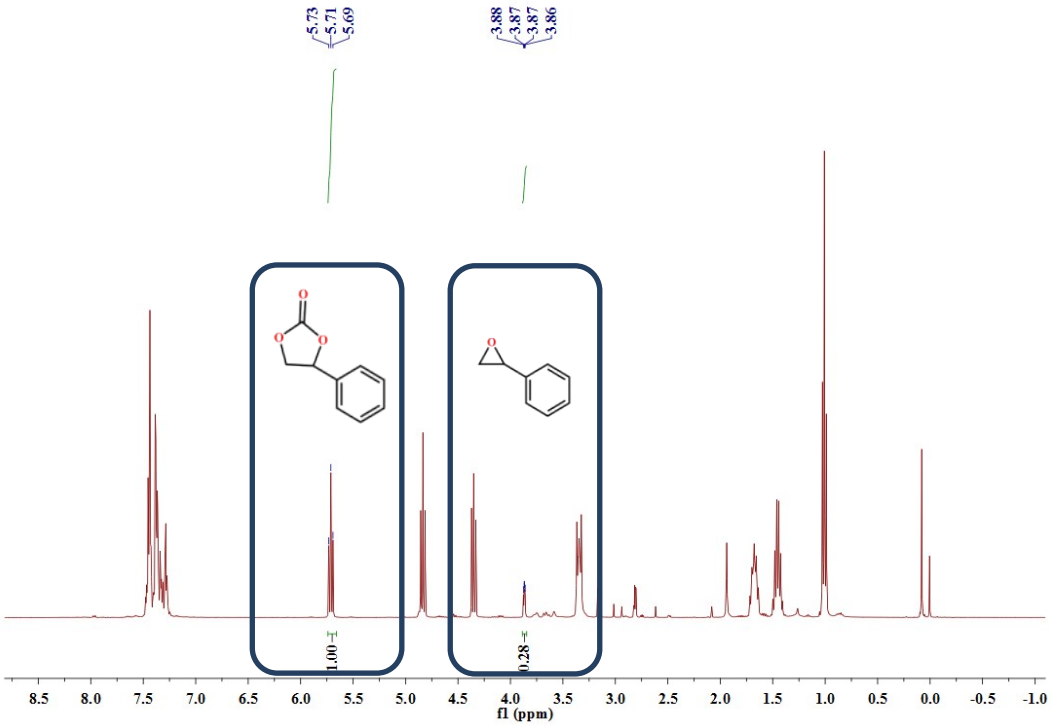

[1] H NMR spectrum of cyclic carbonate with **2a** (Table 1, entry 7).

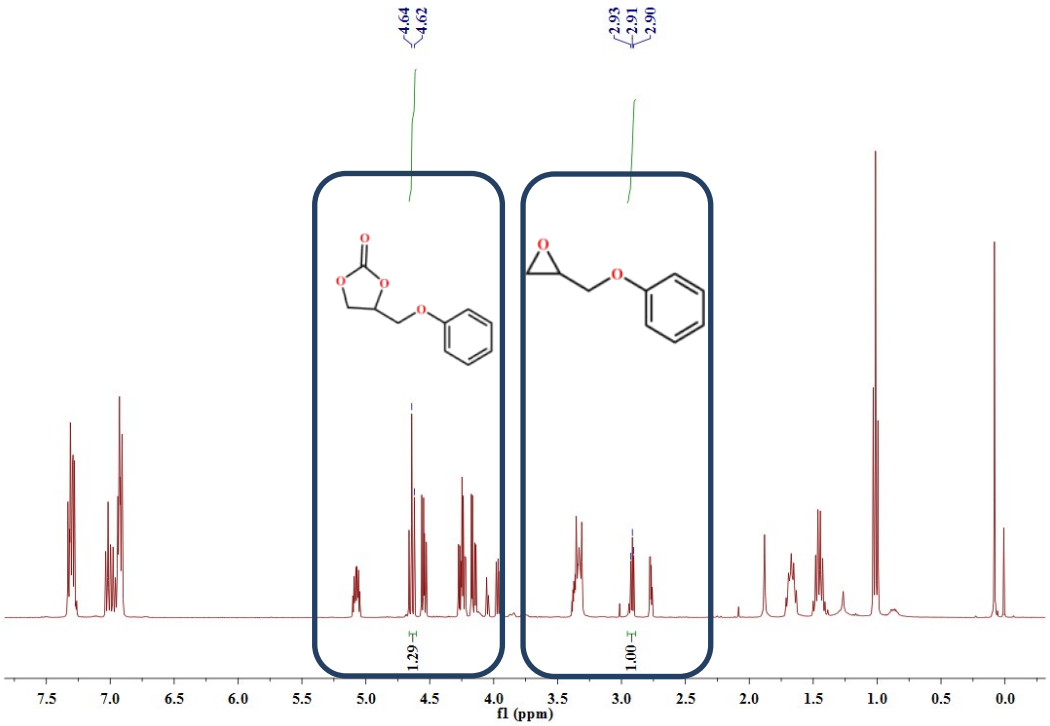

[1] H NMR spectrum of cyclic carbonate with **2a** (Table 1, entry 8).

REFERENCES

(1) D. Bai, Y. Wang, M. He, X Gao and Y. He, *Inorg. Chem. Front.*, 2018, **5**, 2227-2237.

(2) G. Verma, S. Kumar, T. Pham, Z. Niu, L. Wojtas, J. A. Perman, Y.-S. Ch and S. Ma, *Cryst. Growth Des.*, 2017, **17**, 2711-2717.

(3) Y.-Z. Li, H.-H. Yang, H.-Y. Wang, L. Hou, Y.-Y. Wang and Z. Zhu, *Chem. Eur. J.*, 2018, 24, 865–871.

(4) W.-Q. Zhang, R.-D. Wang, Z.-B. Wu, Y.-F. Kang, Y.-P. Fan, X.-Q. Liang, P. Liu and Y.-Y. Wang, *Inorg. Chem.*, 2018, **57**, 1455-1463.

(5) W.-Q. Zhang, R.-D. Wang, Z.-B. Wu, Y.-F. Kang, Y.-P. Fan, X.-Q. Liang, P. Liu and Y.-Y. Wang, *Inorg. Chem.*, 2018, **57**, 1455-1463.

(6) B. Liu, S. Yao, X. Liu, X. Li, R. Krishna, G. Li, Q. Huo and Y. Liu, A*CS Appl. Mater Interfaces*, 2017, **9**, 32820-32828.

(7) Z. Xiang, X. Peng, X. Cheng, X. Li and D. Cao, *J. Phys. Chem. C*., 2011, **115**, 19864–19871.

(8) J. Sim, H. Yim, N. Ko, S. B. Choi, Y. Oh, H. J. Park, S. Park and J. Kim, *Dalton Trans.*, 2014, **43**, 18017–18024.

(9) Y. Yan, M. Jurícek, F.-X. Coudert, N. A. Vermeulen, S. Grunder, A. Dailly, W. Lewis, A. J.

Blake, J. F. Stoddart and M. J. Schröder, *J. Am. Chem. Soc.*, 2016, **138**, 3371-3381.

(10) B. Liu, H.-F. Zhou, L. Hou and Y.-Y. Wang, *Dalton Trans.*, 2018, **47**, 5298–5303.

(11) M. Zhang, Z. Qi, ,Y. Feng, B. Guo, Y. Hao, Z. Xu, L. Zhang and D. Sun, *Chem. Front.*, 2018, **5**, 1314-1320.

(12) B. Wang, A. P. Côté, H. Furukawa, M. O'Keeffe and O. M. Yaghi, *Nature* 2008, **453**, 207-212.

(13) K.-S. Lin, A. K. Adhikari, C.-N. Ku, C.-L. Chiang and H. Kuo, *Int. J. Hydrogen Energy*, **2012**, 37, 13865-13871.